Computergraphical Model for Underwater Image Simulation and Restoration

Thomas Stephan*
*Vision and Fusion Laboratory(IES)
Institute for Anthropomatics
Karlsruhe Institute of Technology
Adenauerring 4, Karlsruhe 76331, Germany
Email: thomas.stephan@kit.edu

Jürgen Beyerer*†
†Fraunhofer IOSB
Fraunhoferstr. 1, Karlsruhe 76331, Germany
Email: juergen.beyerer@iosb.fraunhofer.de

***Abstract*—Visual imaging under water is characterized by low range of visibility and poor image quality. Light interacts with water and its inherent particles in the form of absorption and scattering, causing image degradations, which have to by considered by underwater imaging systems. This can be done by optimizing the image acquisition and image post processing with respect to the properties of water and scene. Therefore a physically based computer graphical model is presented which describes the occurring effects of blurring, loss of contrast, color shift and brightening through backscattering. This model can be used for both: efficient simulation of underwater images and model based image restoration. Furthermore, the presented model can be used to answer theoretical questions on visibility range and imaging performance.**

I. Introduction

Digital Imaging and image processing have been established in a wide range of challenging topics, in surveillance tasks, industrial quality assurance, inspection applications and exploration. All over the world and even in cosmic space optical imaging sensors became very popular. The reason therefore is the human interpretability of visual information. In underwater tasks visual sensor systems are paid little attention. Acoustical sensor systems are the means of choice. Imaging systems under water give only poor results in terms of image quality. That's because of water and its inherent particles interact with light resulting in absorption and scattering and thus in image degradations. Nevertheless, a growing demand on oceanic resources will make visual information of underwater scenery essential in the future. Several underwater tasks in inspection, surveillance and exploration cannot be done without visual information like texture and color. Through the worldwide population increase aqua-farming, oceanic mineral resources like manganese nodules and marine infrastructure like offshore wind parks become more and more important. These all are reasons for an increase of visual imagery systems in future.

But a waterproof housing of camera systems cannot solve the imaging task alone. Optical sensor systems have to cope with many imaging problems. Low light intensities, color shifts, dazzling by backscattering, loss of contrast and blurring reduce the visibility range and the image quality. The result of underwater imagery highly depends on the scenery and on the way to illuminate that scenery. Though, imaging systems for underwater tasks have to be designed by computational imaging aspects: One has to regard both, image acquisition and image processing together.

Creating an underwater imaging system considering only image post processing without regarding integrated image acquisition and lightening, as it was done by most image enhancement and restoration approaches in the past, mostly do not lead to generalizable imaging systems. Otherwise, planning acquisition process and lightening without designing image processing do not result in accurate images either. A very accurate underwater imaging system has to be conceptualized by optimizing both aspects. Therefore, an underwater imagery model is needed, which is able to explain image acquisition process and lightening. A model, which can answer the theoretical questions of visibility range and which can be used for image post processing like image restoration.

A. Related Works

In the 60s and the 70s of the last century essentials of light transportation in scattering medium has been researched [1]–[3]. The radiative transfer equation (RTE) [1] has been developed, which is the fundamental of the physical model of underwater imaging process. Thereof different suitable simulation models were derived, which could be used for simulation of underwater images. The models of Jaffe [4] and McGlamery [5] are based on a small-angle-approximation, which can be used to calculate the point-spread-function (PSF) assuming the phase-function to be small angled. With the aid of a heuristic part, backscattering is also modeled in this approach. These models can be used to synthesize underwater images considering different degradation effects like loss of contrast, brightening by backscatter, blurring and color shift. Furthermore this model is very general and can be used in most underwater tasks without violating inherent assumptions. However, this model also has some disadvantages. The backscattering part is modeled heuristically without considering the real properties of backscattering. This implicit shaped model cannot easily be used for image restoration tasks. Another approach to model underwater imagery was developed by Hou et. al. [6]. They measured real PSFs in different distances and different turbidities and fitted a parametric model. Thus PSF can be easily described by a parametric model. This model can be used in terms of image restoration, but it is limited by implicit assumptions concerning lightening, scenery and water inherent properties. In the last few years many image enhancement and image restoration approaches have been developed [7]. Thereby, heuristically image enhancement methods [8], [9] can produce impressive quality results, but they are restricted by its implicit assumptions and therefore, can only be used under constrained lightening conditions. Many developed image and color restoration methods are based on a simplified imaging model

$$\boldsymbol{I}(x) = \boldsymbol{J}(x)t(x) + \boldsymbol{A} \cdot (1 - t(x)) \ , \tag{1}$$

where $\boldsymbol{I}(x)$ is the observed color vector, $\boldsymbol{J}(x)$ is the scene radiance, $\boldsymbol{A}$ is the global atmospheric light and $t(x)$ is the medium transmission. This model is often used with assumptions like the dark channel prior [10]. These approaches [11]–[13], based on (1) contain a strong assumption as shown in [11]: Global homogeneous lightening. Thus, they only can be used under very special conditions. These models cannot handle other illumination types like artificial illumination.

B. This Paper

Today, computer graphical methods are the means of choice for visual simulation and modeling tasks. They can be used to synthesize photorealistic imaging results, taking into account mostly every optical effect. But, using the whole range of photorealistic rendering is of computational complexity and therefore expensive in terms of computational performance. To model underwater imaging processes, using all these methods is quite oversized from practical point of view. In this paper a model is presented, which is based on the computer graphical recursive rendering equation adapted onto underwater imagery by using specific properties and assumptions, which are mostly fulfilled. Hence, this model can be used for efficient simulation and theoretical issues, also visibility ranges dependent on the water properties and for image restoration methods.

First the fundamentals of the recursive rendering equation will be described in II-A. Afterwards the new imaging model will be described in II-B, presented in a clear mathematical formulation as affine transformation (II-C) and then be discussed in II-D.

II. Underwater Imaging Model

Using computer graphics for simulating photorealistic images is common practice. Nevertheless, modeling and simulating participating medium like scattering water or haze is still a major challenge in computer graphical research [14], [15]. All computer graphic render approaches are based on the recursive rendering equation.

A. Recursive Rendering Equation

The rendering equation [16], [17] was developed in 1986 by David S. Immel et al. and James T. Kajiya. In this recursive integral equation, the radiance L_o leaving a point $\boldsymbol{x}$ into direction r_o is given by the sum of emitted radiance L_e and reflected radiance L_i.

$$L_o(\boldsymbol{x}, \boldsymbol{r}_o) = L_e(\boldsymbol{x}, \boldsymbol{r}_o) + \int_{\mathcal{S}^2} \rho(\boldsymbol{x}, \boldsymbol{r}_i, \boldsymbol{r}_o) L_i(\boldsymbol{x}, \boldsymbol{r}_i) \langle \boldsymbol{r}_i, \boldsymbol{n} \rangle \, \mathrm{d}\boldsymbol{r}_i \ , \tag{2}$$

where $\boldsymbol{r} \in \mathcal{S}^2 = \left\{ \boldsymbol{r} \in \mathbb{R}^3 | \, \|\boldsymbol{r}\| = 1 \right\}$is a normalized direction, $\rho(\cdot)$ is the bidirectional reflectance distribution function (BRDF) depending on the direction of ingoing radiance $\boldsymbol{r}_i$ and of outgoing radiance $\boldsymbol{r}_o$ and $\langle \boldsymbol{r}_i, \boldsymbol{n} \rangle$ is the cosine angle of the ingoing radiance and the normalized surface normal $\boldsymbol{n}$. Fig. 1 illustrates the disposal of the used variables.

The problem is the recursive character and the computational

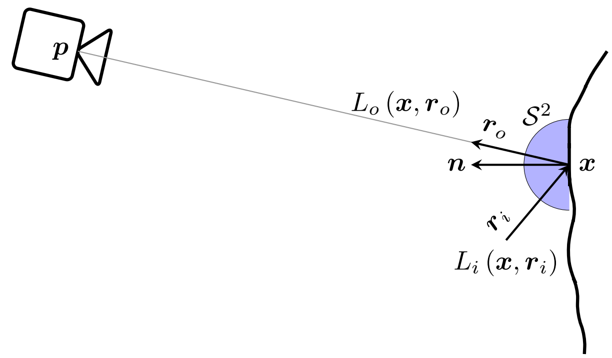

Fig. 1: Radiance $L_o(\boldsymbol{x}, \boldsymbol{r}_o)$ reflected by object surface point $\boldsymbol{x}$ can be calculated by weighted integration (2) of incoming radiation $L_i(\boldsymbol{x}, \boldsymbol{r}_i)$ at $\boldsymbol{x}$

expensive integration. The ingoing radiance $L_i(\boldsymbol{x}, \boldsymbol{r}_i)$ can then again be caused by reflection of light at another position $\boldsymbol{x}'$. Thus, modern render algorithms must solve two important problems. Choosing recursion depth depends on scenery, reflectance and lightening and chosen integration algorithm. Out of this, quite different approaches have been developed for different field of use. Examples therefore are photon mapping [18], path tracing, bidirectional path tracing [19], metropolis light transport [20] and many more.

Whereby, assuming light rays travelling through empty space without any change, rendering in participating medium is much more computational complex. Therefore, one has to consider light interaction in medium. This can be done by the transport equation [15], [21]

$$L_o(\boldsymbol{x}, \boldsymbol{r}_o) = \int_0^\infty T(\boldsymbol{x}, \boldsymbol{x} + \tau \boldsymbol{r}_o) L_s(\boldsymbol{x} + \tau \boldsymbol{r}_o, -\boldsymbol{r}_o) \mathrm{d}\tau \ , \tag{3}$$

where $T(\cdot)$ can be calculated by

$$T(\boldsymbol{x}, \boldsymbol{x} + \tau \boldsymbol{r}_o) = \exp\left(-\int_0^\tau c(\boldsymbol{x} + \tau' \boldsymbol{r}_o) \mathrm{d}\tau' \right) \ , \tag{4}$$

where $c(\boldsymbol{x}) = a(\boldsymbol{x}) + b(\boldsymbol{x})$ is the extinction coefficient, which is the sum of the absorption coefficient $a(\boldsymbol{x})$ and the scattering coefficient $b(\boldsymbol{x})$.

Assuming a homogeneous medium $T(\cdot)$ degenerates to the attenuation factor $T(\boldsymbol{x}, \boldsymbol{z}) = \exp\left(-c \left\|\boldsymbol{x} - \boldsymbol{z}\right\|\right)$ of the Beer-Lambert law. $L_s(\boldsymbol{x}_\tau, \boldsymbol{r}_o)$ is the radiation caused by inscattering and can be calculated by

$$L_s(\boldsymbol{x}_\tau, \boldsymbol{r}_o) = L_e(\boldsymbol{x}_\tau, \boldsymbol{r}_o) + \int_{\mathcal{S}^2} \beta\left(\boldsymbol{x}_\tau, \langle \boldsymbol{r}_o, -\boldsymbol{r}_i \rangle\right) L_i(\boldsymbol{x}_\tau, \boldsymbol{r}_i) \mathrm{d}\boldsymbol{r}_i \ , \tag{5}$$

where L_e is the emitted radiation and $\beta(\cdot)$ is the so called phase function, which describes the scattering distribution dependent on the cosine of the scattering angle. L_i can be calculated recursively with (2) and (5). For better understanding, Fig.2 illustrates the volume rendering setting.

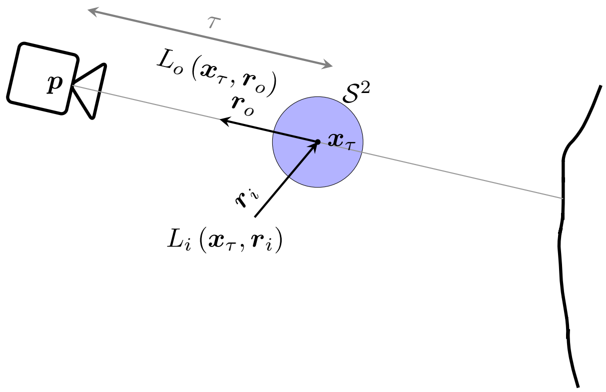

Fig. 2: Radiance $L_o(\boldsymbol{x}_\tau, \boldsymbol{r}_o)$ scattered by medium at point $\boldsymbol{x}_\tau$ can be calculated by weighted integration (5) of incoming radiation $L_i(\boldsymbol{x}_\tau, \boldsymbol{r}_i)$ at $\boldsymbol{x}_\tau$, where the weights can be calculated by the angle dependent phase function $\beta(\cdot)$.

If camera is modeled as pinhole camera, the pixel intensity can be calculated, by integrating the incoming radiance

$$g \propto \int_{\Omega \subset \mathcal{S}^2} L_i(\boldsymbol{p}, \boldsymbol{r}) \mathrm{d}\boldsymbol{r} \ , \tag{6}$$

where $\boldsymbol{p}$ is the pinhole and $\Omega \subset \mathcal{S}^2$ is the solid angle of the cone, spanned by the projection of the pixel area and the projection center $\boldsymbol{p}$.

B. Computergraphical Model for Underwater Imaging

The challenge of modeling light transportation for underwater imagery lies in the choice of recursion depth, by neglecting light paths with small contribution to the total amount of image intensity. In this approach a single-scattering model will be presented, which is able to explain the common degradations of underwater imaging, like low intensities, loss of contrast, color shift, brightening by backscattering and blurring. Thereby – similar to the model of McGlamery [5] – the total image intensity $g(\boldsymbol{u})$ is split into three different additive components, based on the physical rendering equations. Fig. 3 shows the three different components and the properties of the camera model.

1) Direct Component: The direct component represents the path of light transportation, which goes from the light source to the camera sensor by reflecting at the object surface point without any interaction of medium than by attenuation. This component contains the most information about the object reflectance. This component can be derived from the rendering equation (2) and the transport equation (3) by assuming a homogeneous medium, lambertian reflection $\rho(\boldsymbol{x}, \boldsymbol{r}_i, \boldsymbol{r}_o) = \rho(\boldsymbol{x})$ and a pinhole camera model.

$$g^{\mathrm{dir}}(\boldsymbol{x}) = \int_{\mathcal{A}_{\boldsymbol{x}}} I_{\boldsymbol{\xi}}\left(\widehat{\boldsymbol{x}-\boldsymbol{\xi}}\right) \frac{\rho(\boldsymbol{x})}{\|\boldsymbol{x}-\boldsymbol{p}\|^2 \|\boldsymbol{x}-\boldsymbol{\xi}\|^2} \cdot \left\langle \widehat{\boldsymbol{\xi}-\boldsymbol{x}}, \boldsymbol{n}_{\boldsymbol{x}} \right\rangle e^{-c(\|\boldsymbol{x}-\boldsymbol{\xi}\|+\|\boldsymbol{p}-\boldsymbol{x}\|)} \mathrm{d}\boldsymbol{x} \ , \tag{7}$$

where $I_{\boldsymbol{\xi}}(\widehat{\boldsymbol{r}})$ is the intensity of light source at $\boldsymbol{\xi}$ emitted into the normalized direction $\widehat{\boldsymbol{r}} = \frac{\boldsymbol{r}}{\|\boldsymbol{r}\|}$. $\mathcal{A}_{\boldsymbol{x}}$ is the projected object-sided pixel Area. Fig. 4 shows the arrangement of the scene.

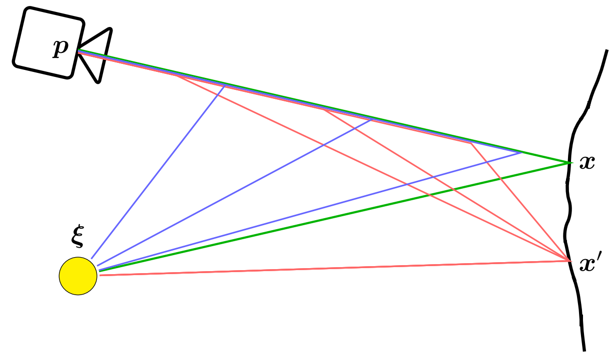

Fig. 3: This figure shows the three considered components of light paths affecting the perceived pixel intensity. The direct component (green line) represents the path of light reflected by the object surface $\boldsymbol{x}$ towards the camera pinhole $\boldsymbol{p}$. The blurring component (red lines) contains all paths, reflected by an object surface point $\boldsymbol{x}'$, which are scattered into the line of sight $\overline{\boldsymbol{p}\boldsymbol{x}}$. The indirect component (blue lines) represents the light rays emitted by the light source and scattered into the line of sight $\overline{\boldsymbol{p}\boldsymbol{x}}$ without being reflected on scene surface.

The direct component can be approximated without intro-

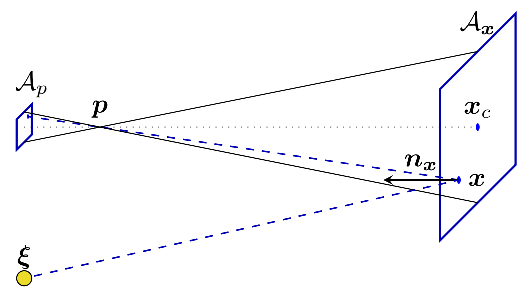

Fig. 4: This figure illustrates the direct component. Light rays emitted by light source $\boldsymbol{\xi}$ are reflected by the scene surface $\boldsymbol{x}$ into direction of the pinhole $\boldsymbol{p}$ of the camera. Radiation has to be integrated over the surface area $\mathcal{A}_{\boldsymbol{x}}$, which is the projection of the pixel area $\mathcal{A}_p$ onto the object surface

ducing major errors by assuming the reflectance $\rho(\boldsymbol{x})$ to be constant over the area $\mathcal{A}_{\boldsymbol{x}}$

$$\widetilde{g}^{\mathrm{dir}}(\boldsymbol{x}) = \frac{|\mathcal{A}_p|}{b^2} I_{\boldsymbol{\xi}}\left(\widehat{\boldsymbol{x}_c-\boldsymbol{\xi}}\right) \frac{\rho(\boldsymbol{x}_c)}{\|\boldsymbol{x}_c-\boldsymbol{\xi}\|^2} \cdot \left\langle \widehat{\boldsymbol{\xi}-\boldsymbol{x}_c}, \boldsymbol{n}_{\boldsymbol{x}_c} \right\rangle e^{-c(\|\boldsymbol{x}_c-\boldsymbol{\xi}\|+\|\boldsymbol{p}-\boldsymbol{x}_c\|)} \ , \tag{8}$$

where $|\mathcal{A}_p|$ is the size of one pixel, b is the distance between the sensor and the pinhole $\boldsymbol{p}$ and $\boldsymbol{x}_c$ is the center point of $\mathcal{A}_{\boldsymbol{x}}$.

2) Blurring Component: The blurring component represents the paths of light transportation, which travel from the light source at $\boldsymbol{\xi}$,these are reflected by an object surface $\boldsymbol{x}'$ and inscattered into the line of sight $\overline{\boldsymbol{p}\boldsymbol{x}}$ at $\boldsymbol{\eta}_\tau$. This component describes how neighboring object points contribute to the total amount of pixel intensity and therefore how much the image will be blurred. This component can be used to PSFs by given water inherent optical properties. Fig. 5 shows the arrangement of the scene.

$$g^{\text{blur}}(\boldsymbol{x},\boldsymbol{x}') = \int_0^{\|\boldsymbol{p}-\boldsymbol{x}_c\|} \int_{\mathcal{A}_{\boldsymbol{x}'}} \int_{\mathcal{A}_{\eta_\tau}} I_{\boldsymbol{\xi}}\left(\widehat{\boldsymbol{x}'-\boldsymbol{\xi}}\right) \cdot \frac{\rho(\boldsymbol{x}')\,\beta\left(\left\langle \widehat{\boldsymbol{x}'-\boldsymbol{\eta}_\tau}, \widehat{\boldsymbol{p}-\boldsymbol{\eta}_\tau}\right\rangle\right)}{\|\boldsymbol{x}'-\boldsymbol{\xi}\|^2\,\|\boldsymbol{\eta}_\tau-\boldsymbol{x}'\|^2\,\|\boldsymbol{p}-\boldsymbol{\eta}_\tau\|^2} \left\langle \widehat{\boldsymbol{\xi}-\boldsymbol{x}'}, \boldsymbol{n}_{\boldsymbol{x}'}\right\rangle \cdot e^{-c\left(\|\boldsymbol{x}'-\boldsymbol{\xi}\|+\|\boldsymbol{\eta}_\tau-\boldsymbol{x}'\|+\|\boldsymbol{p}-\boldsymbol{\eta}_\tau\|\right)} \mathrm{d}\boldsymbol{\eta}_\tau \mathrm{d}\boldsymbol{x}' \mathrm{d}\tau \;, \tag{9}$$

where $\mathcal{A}_\eta$ is slice of the cone spanned by the projected pixel perpendicular to the sight line $\overline{\boldsymbol{p}\,\boldsymbol{x}_c}$. $\beta(\cos(\alpha))$ is the so called phase function and describes the angle dependent scattering distribution. This equation also can be approximated according to (8)

$$\widetilde{g}^{\text{blur}}(\boldsymbol{x},\boldsymbol{x}') = \|\boldsymbol{p}-\boldsymbol{x}_c\|^2 \frac{|\mathcal{A}_p|^2}{b^4} \int_0^{\|\boldsymbol{p}-\boldsymbol{x}_c\|} I_{\boldsymbol{\xi}}\left(\widehat{\boldsymbol{x}_c'-\boldsymbol{\xi}}\right) \cdot \frac{\rho(\boldsymbol{x}_c')\,\beta\left(\left\langle \widehat{\boldsymbol{x}_c'-\boldsymbol{\eta}_c}, \widehat{\boldsymbol{p}-\boldsymbol{\eta}_c}\right\rangle\right)}{\|\boldsymbol{x}_c'-\boldsymbol{\xi}\|^2\,\|\boldsymbol{\eta}_c-\boldsymbol{x}_c'\|^2} \left\langle \widehat{\boldsymbol{\xi}-\boldsymbol{x}_c'}, \boldsymbol{n}_{\boldsymbol{x}_c'}\right\rangle \cdot e^{-c\left(\|\boldsymbol{x}_c'-\boldsymbol{\xi}\|+\|\boldsymbol{\eta}_c-\boldsymbol{x}_c'\|+\tau\right)} \mathrm{d}\tau \;, \tag{10}$$

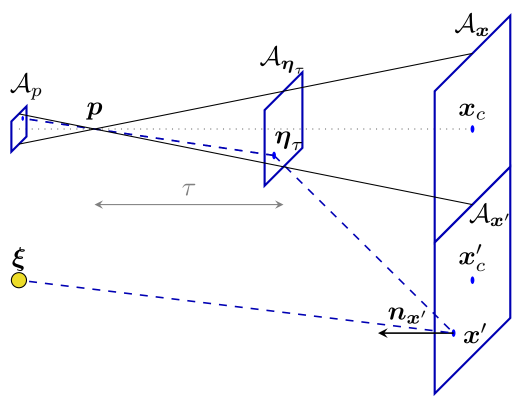

Fig. 5: The blurring component describes how neighboring pixels affects the perceived pixel intensity. A surface area $\mathcal{A}_{\boldsymbol{x}'}$ is illuminated by the light source $\boldsymbol{\xi}$. The reflected light travels through the medium and is scattered at $\boldsymbol{\eta}_\tau$ into direction of pinhole $\boldsymbol{p}$, whereby $\boldsymbol{\eta}_\tau$ is inside the cone, spanned by the projection of the pixel area $\mathcal{A}_p$. Radiation have to be integrated over the object surface $\mathcal{A}_{\boldsymbol{x}'}$ and over each point into the spanned cone. Hereby, $\mathcal{A}_{\boldsymbol{x}'}$ is the projection of another pixel.

3) Indirect Component: The indirect component represents the paths of light transportation, which are traveling from the light source at $\boldsymbol{\xi}$ and are inscattered into the line of sight $\overline{\boldsymbol{p}\,\boldsymbol{x}}$ at $\boldsymbol{\eta}_\tau$ without reflection at any object surface. This component is an additive part without any object reflectance information (Fig.6). It causes image brightening and loss of contrast. The indirect component increases monotonically with the distance to the object surface. It can be calculated by

$$g^{\text{ind}}(\boldsymbol{x}) = \int_0^{\|\boldsymbol{p}-\boldsymbol{x}_c\|} \int_{\mathcal{A}_{\eta_\tau}} I_{\boldsymbol{\xi}}\left(\widehat{\boldsymbol{\eta}_\tau-\boldsymbol{\xi}}\right) \cdot \frac{\beta\left(\left\langle \widehat{\boldsymbol{\eta}_\tau-\boldsymbol{\xi}}, \widehat{\boldsymbol{p}-\boldsymbol{\eta}_\tau}\right\rangle\right)}{\|\boldsymbol{\eta}_\tau-\boldsymbol{\xi}\|^2\,\|\boldsymbol{p}-\boldsymbol{\eta}_\tau\|^2} e^{-c(\|\boldsymbol{\eta}_\tau-\boldsymbol{\xi}\|+\|\boldsymbol{p}-\boldsymbol{\eta}_\tau\|)} \mathrm{d}\boldsymbol{\eta}_\tau \mathrm{d}\tau \tag{11}$$

and be approximated by

$$\widetilde{g}^{\text{ind}}(\boldsymbol{x}) = \frac{|\mathcal{A}_p|}{b^2} \int_0^{\|\boldsymbol{p}-\boldsymbol{x}_c\|} I_{\boldsymbol{\xi}}\left(\widehat{\boldsymbol{\eta}_c-\boldsymbol{\xi}}\right) \cdot \frac{\beta\left(\left\langle \widehat{\boldsymbol{\eta}_c-\boldsymbol{\xi}}, \widehat{\boldsymbol{p}-\boldsymbol{\eta}_c}\right\rangle\right)}{\|\boldsymbol{\eta}_c-\boldsymbol{\xi}\|^2} e^{-c(\|\boldsymbol{\eta}_c-\boldsymbol{\xi}\|+\|\boldsymbol{p}-\boldsymbol{\eta}_c\|)} \mathrm{d}\tau \tag{12}$$

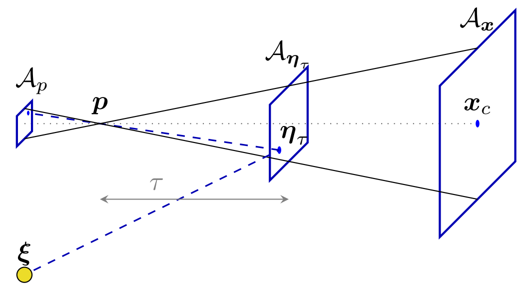

Fig. 6: The indirect component adds intensity to the perceived pixel, which contains no information of the object reflectance. Light, emitted by the light source $\boldsymbol{\xi}$ is scattered at $\boldsymbol{\eta}$ towards the pinhole $\boldsymbol{p}$, whereby $\boldsymbol{\eta}$ lies inside the cone, spanned by the projection of the pixel area $\mathcal{A}_p$. To get the whole amount of the indirect component, radiation has to be integrated over the spanned cone.

C. Affine Transformation

These three components can be subsumed to one affine transformation containing the direct, blurring and indirect component. Thereby the image $\boldsymbol{g}$ is represented as vector containing every pixel intensity. The affine transformation is

$$\boldsymbol{g} = \Gamma\boldsymbol{\rho} + \boldsymbol{b} \;, \tag{13}$$

where $\boldsymbol{\rho}$ is the reflectance vector containing the object surface reflectance to the corresponding pixels. The matrix $\Gamma = \Gamma^{\text{dir}} + \Gamma^{\text{blur}}$ is the sum of the direct and the blurring transfer function. $\boldsymbol{b}$ represents the indirect component, which does not interact with the object surface reflectance.

$$\begin{aligned} \Gamma^{\text{dir}} &= \left(\gamma_{ij}^{\text{dir}}\right) && \text{with} \\ \gamma_{ii}^{\text{dir}} &= \frac{\widetilde{g}^{\text{dir}}(\boldsymbol{x}_i)}{\rho(\boldsymbol{x}_i)} && \text{and} \\ \gamma_{ij}^{\text{dir}} &= 0 && \text{where } i \neq j \end{aligned} \tag{14}$$

is a diagonal Matrix. Γ^{blur} has a block like structure just as other space variant transfer functions in computer vision [22], its elements are

$$\gamma_{ij}^{\text{blur}} = \frac{\widetilde{g}^{\text{blur}}(\boldsymbol{x}_i,\boldsymbol{x}_j)}{\rho(\boldsymbol{x}_j)} \;. \tag{15}$$

Dependent on the width of the blurring kernel, Γ is sparsely populated.

D. Model Discussion

Every model raises the question of its reliability in a given environment. The mainly restricting assumption of the proposed model is the single-scattering assumption. Thus, in our case, this leads to the question whether the single-scattering model is sufficient for underwater imaging processing. In order to discuss this, the quantity of *optical thickness* will be introduced. Optical thickness or optical depth is the multiplication of distance (in meter) and extinction coefficient $c[\frac{1}{m}]$ and as a consequence it is dimensionless. The quantity of optical thickness also has a physical meaning. The stochastic mean path length, which a 'photon' travels through water without being scattered or absorbed is exactly one optical depth [23]. The distance, where on average the first scattering or absorption event takes place, is at one optical depth, the second scattering event nearly at two optical depths. As a consequence, the contribution to imaging process decreases with the number of scattering events, if the target distance is less than one optical depth. Fig. 7 illustrates the decrease of the total contribution of image intensity due to the number of scattering events for different distances.

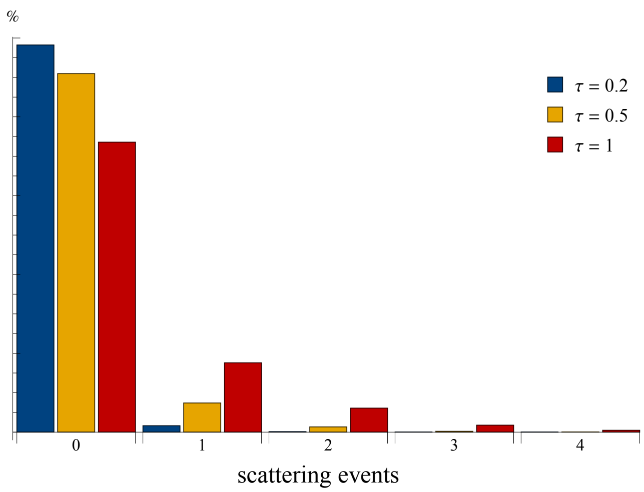

Fig. 7: This plot shows the contribution – determined by monte-carlo simulation – to the total image pixel intensity due to the number of scattering events and target distances (blue: $\tau = 0.2$, yellow: $\tau = 0.5$, red: $\tau = 1.0$).

Furthermore, scattering events fan out light beams resulting in enlarged PSF parts. As a consequence the intensity caused by multiple scattering distributes to a wider area. As a result, the peak to peak ratio of the PSF caused by multiple scattering and the PSF caused by single scattering is often less than the sensor sensibility (Fig. 8). Therefor, multiple scattering has only a slight impact on the imaging process for distances less than one optical depth.

Thus, this model is sufficient for underwater vision tasks at the minimum up to one optical depth. Acquired images as part of a series of underwater imaging tests has shown, that it is hardly possible to perceive anything in more than one optical depth. For illustration purpose some images of this series is shown in Fig.9

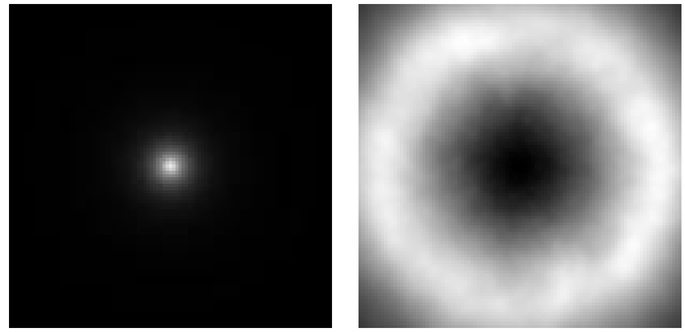

(a) single-scattering PSF (b) double-scattering PSF

Fig. 8: Simulated PSF parts, caused by single-scattering (left) and double-scattering (right) in a distance of one optical depth ($\tau = 1$). These results were simulated by monte-carlo simulation. For the purpose of visibility PSF caused by double-scattering is brightened up. The peak to peak ratios are 0.51% for the single-scattering PSF and 0.015% for the double-scattering PSF compared to the direct component. Hence, parts of PSF, caused by multiple scattering has only slight impact to the total PSF.

III. Simulation

The purpose of simulation often is to plan and design underwater imaging systems. Such systems are very expensive and the cost increase with the water depth in which it will be applied. Furthermore, producing an underwater imaging system is very time-consuming, because there is only a limited market of underwater components; which is why many components of such systems are self-elaborated. Thus, it is not be able to afford to create a system, which gives only poor imaging results. Simulation of imaging systems can be done before creating systems in hardware to optimize configuration of lightening and imaging in advance, in order to reduce costs.

The proposed model can be used to simulate underwater images. It can be calculated very efficiently by GPU parallelization and rasterization techniques. The components (direct, blurring and indirect) can be calculated separately, whereby different effects can also be rated separately. Thus, loss of intensity and color shifts condenses very apparently in the direct and blurring component, brightening through backscattering and loss of contrast can be seen at the indirect component and the amount and strength of blurring is part of the blurring component. Lightening for example can be optimized on the basis of direct and indirect component, whereas blurring barely depends on position of light sources, but on existing water properties. Fig. 10 shows a simulated example and its three components. The potential of computational efficiency of the proposed method make an automated optimization possible. Lightening parameters, such as light positions and light shape characteristics can be optimized to get better imaging results.

Simulation results also can be used to implement and validate image enhancement and image restoration approaches. To objectively verify image post processing methods one has to know the original object reflectance to compare it with the processed image. Getting ground truth data about scene properties and surface reflectance is a difficult task.

Changing water inherent properties in a desired manner is nearly impossible. In this cases, simulation is unavoidable.

IV. Restoration

Underwater image restoration is an inverse problem, which is ill-posed. As a consequence the image process cannot be inverted naively; otherwise restoration results are dominated by unpleasing artifacts. Model inverting must be regularized. Solving ill-posed problems by regularization can be very complex, but there is a mathematical domain, in which ill-posedness is studied very well [24]. These are linear problems. Within this domain there are different regularization methods. In spectral domain these are for example truncated singular value decomposition (TSVD), Tikhonov regularization and the Wiener filter. Other popular methods are the Richardson-Lucy algorithm, steepest descent and total variation approaches. The formulation of the proposed model as affine image model can be used for image restoration in a conventional way. Blind deconvolution approaches can also be used to perform restoration results by shaping a-priori knowledge about the PSF. First experiments of image restoration based on the proposed method perform promising restoration results. Fig. 11 shows some restoration results based on this model.

V. Conclusion

The introduced model has many advantages against other existing underwater imaging models. It can be calculated more efficiently than oversized computer graphical techniques, which do not fully consider the properties of underwater imaging. However it is more accurate than existing underwater imaging models and can be extended by adding multi-scattering components. This model can be used for a wide range of underwater sceneries and is not restricted by strong assumptions on lightening. Therefore, the range of application is wider than by existing models, it also can be used for automatized image post-processing workflows. It enables another access to theoretical questions on visibility range, lightening techniques and image post-processing. modeling underwater imaging as affine transformation has outstanding benefits. This formulation can be used in standard image restoration approaches. Restoration techniques like Tikhonov filter, Wiener filter and total variation filter can be adapted easily to underwater vision tasks.

References

[1] S. Chandrasekhar, *Radiative transfer*. New York: Dover, 1960.

[2] A. Ishimaru, *Wave propagation and scattering in random media*. New York: Academic Pr., 1978.

[3] ——, "Pulse propagation, scattering, and diffusion in scatterers and turbulence," *Radio Science*, vol. 14, no. 2, pp. 269–276, 1979.

[4] J. S. Jaffe, "Computer Modeling and the Design of Optimal Underwater Imaging Systems," *Oceanic Engineering, IEEE Journal of*, vol. 15, no. 2, pp. 101–111, 1990.

[5] B. L. McGlamery, "A computer model for underwater camera systems," *Ocean Optics*, no. 208, 1979.

[6] W. Hou, D. J. Gray, and A. D. Weidemann, "Automated underwater image restoration and retrieval of related optical properties," *Geoscience and Remote Sensing Symposium, 2007. IGARSS 2007. IEEE International*, pp. 1889–1892, 2007.

[7] S. Raimondo and C. Silvia, "Underwater image processing: state of the art of restoration and image enhancement methods," *EURASIP Journal on Advances in Signal Processing*, vol. 2010, 2010.

[8] A. T. Çelebi and S. Ertürk, "Visual enhancement of underwater images using Empirical Mode Decomposition," *Expert Systems with Applications*, vol. 39, no. 1, pp. 800–805, 2012.

[9] M. Chambah, D. Semani, A. Renouf, P. Courtellemont, and A. Rizzi, "Underwater Color Constancy: Enhancement of Automatic Live Fish Recognition," *IS&T*, vol. 2004, 2004.

[10] K. He, J. Sun, and X. Tang, "Single image haze removal using dark channel prior," *Pattern Analysis and Machine Intelligence, IEEE Transactions on*, vol. 33, no. 12, pp. 2341–2353, 2011.

[11] T. Stephan, P. Frühberger, S. Werling, and M. Heizmann, "Model based image restoration for underwater images," in *SPIE Optical Metrology 2013*. International Society for Optics and Photonics, 2013, pp. 87 911F–87 911F.

[12] J. Y. Chiang and Y.-C. Chen, "Underwater Image Enhancement by Wavelength Compensation and Dehazing," *Image Processing, IEEE Transactions on*, vol. 21, no. 4, pp. 1756–1769, 2012.

[13] K. He, J. Sun, and X. Tang, "Single Image Haze Removal Using Dark Channel Prior," *IEEE Transactions on Pattern Analysis and Machine Intelligence*, 2010.

[14] J. Novák, D. Nowrouzezahrai, C. Dachsbacher, and W. Jarosz, "Virtual ray lights for rendering scenes with participating media," *ACM Transactions on Graphics (TOG)*, vol. 31, no. 4, p. 60, 2012.

[15] T. Engelhardt, J. Novak, and C. Dachsbacher, "Instant multiple scattering for interactive rendering of heterogeneous participating media," *Karlsruhe Institut of Technology, Tech. Rep*, 2010.

[16] D. S. Immel, M. F. Cohen, and D. P. Greenberg, "A radiosity method for non-diffuse environments," *ACM SIGGRAPH Computer Graphics*, vol. 20, no. 4, pp. 133–142, 1986.

[17] J. T. Kajiya, "The rendering equation," in *ACM Siggraph Computer Graphics*, vol. 20, no. 4. ACM, 1986, pp. 143–150.

[18] H. W. Jensen, *Realistic image synthesis using photon mapping*. AK Peters, Ltd., 2001.

[19] E. P. Lafortune and Y. D. Willems, "Bi-directional path tracing," in *Proceedings of CompuGraphics*, vol. 93, 1993, pp. 145–153.

[20] E. Veach and L. J. Guibas, "Metropolis light transport," in *Proceedings of the 24th annual conference on Computer graphics and interactive techniques*. ACM Press/Addison-Wesley Publishing Co., 1997, pp. 65–76.

[21] T. Engelhardt and C. Dachsbacher, "Epipolar sampling for shadows and crepuscular rays in participating media with single scattering," in *Proceedings of the 2010 ACM SIGGRAPH symposium on Interactive 3D Graphics and Games*. ACM, 2010, pp. 119–125.

[22] B. K. Gunturk and X. Li, *Image restoration: Fundamentals and advances*, ser. Digital imaging and computer vision. Boca Raton and FL: CRC Press, 2013.

[23] C. D. Mobley, *Light and water: Radiative transfer in natural waters*. San Diego: Academic Press, 1994.

[24] A. Rieder, *Keine Probleme mit inversen Problemen: Eine Einführung in ihre stabile Lösung ; [mit Online-Service zum Buch]*, 1st ed. Wiesbaden: Vieweg, 2003.

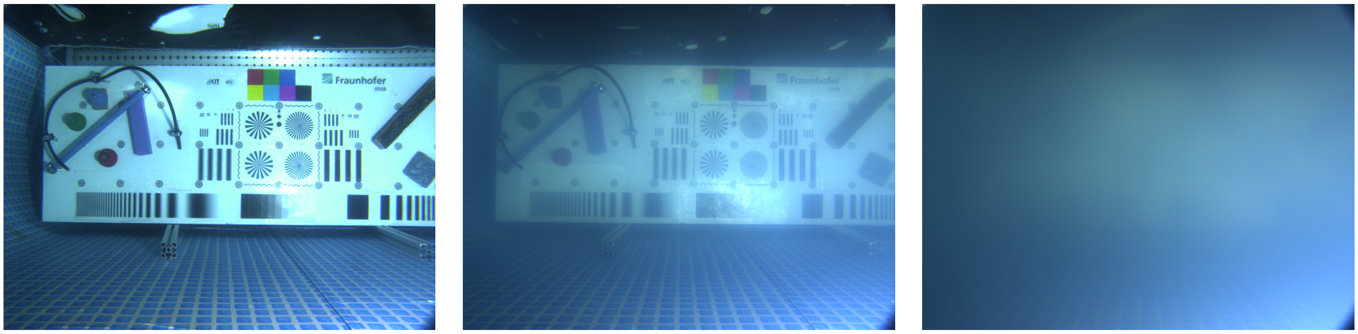

(a) $\tau = 0.2$ (b) $\tau = 0.48$ (c) $\tau = 0.9$

Fig. 9: This images figure the visibility decrease with decreasing optical thickness. The seen target is positioned in a distance of $1.5m$. With increasing turbidity optical thickness also increase (from $\tau = 0.2$ over $\tau = 0.48$ to $\tau = 0.9$). In small optical distances the target can be perceived very accurately, in contrast even the surrounding of the target at $\tau = 0.9$ can hardly be seen. Underwater image acquisition is mainly useful below a distance of one optical depth. Thus, the single-scattering assumption matches very well for underwater imaging tasks.

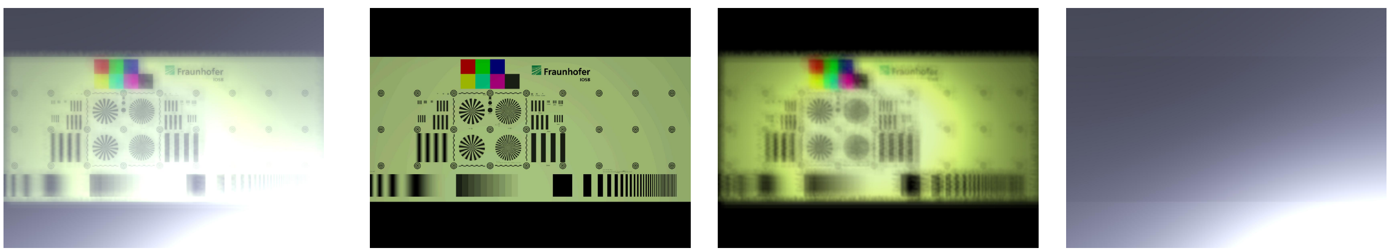

(a) Simulation (b) Direct component (c) Blurring component (d) Indirect component

Fig. 10: This figure shows an underwater simulation based on the proposed model (for the purpose of visibility the direct and the blurring component have been brightened up). The Simulation result (left image) is the sum of direct, blurring and indirect component (from left to right). Color-shift can be seen at the direct and the blurring component, where the brightening caused through backscattering shows up in the indirect component.

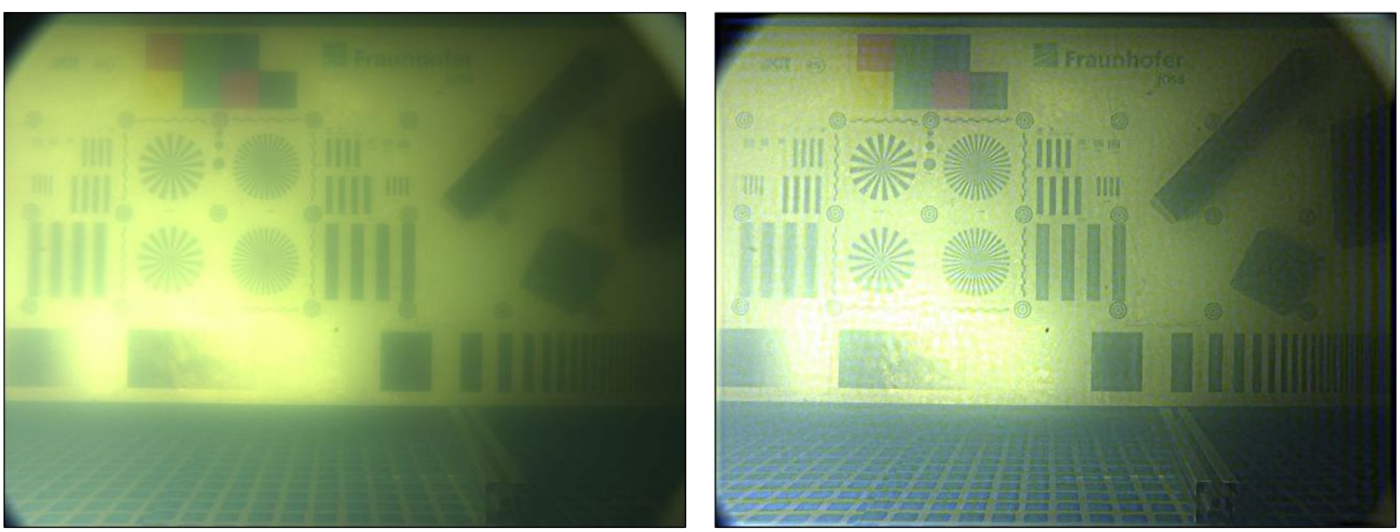

Fig. 11: This figure shows first experimental results of image restoration on real – non-simulated – images, based on the proposed model. For image restoration a total variation approach has been used, where the kernel was calculated by evaluating the blurring component (10). As a consequence the image could be sharpened, hence, details are more visible, which can be seen especially at the concentric circles.